SciMedCentral

JSM Nanotechnology & Nanomedicine

Research Article

Selection for Ionic- Confers Silver Nanoparticle Resistance in *Escherichia coli*

Mehrdad Tajkarimi[1], Kristen Rhinehardt[2,5], Misty Thomas[3,5], Jude Akamu Ewunkem[2,5], Adero Campbell[2,5], Sada Boyd[4,5], Devana Turner[3], Scott H. Harrison[3,5], and Joseph L. Graves Jr[2,5]*

[1]*Brentwood Biomedical Research Institute, Los Angeles, CA 90073, USA*

[2]*Department of Nanoengineering, North Carolina A&T State University & UNC Greensboro, USA*

[3]*Department of Biology, North Carolina A&T State University, USA*

[4]*Department of Energy and Environment, North Carolina A&T State University, USA*

[5]*Beacon Center for the Study of Evolution in Action, USA*

***Corresponding author**

Joseph L. Graves Jr, Joint School of Nanoscience & Nanoengineering, North Carolina A&T State University and UNC Greensboro, Greensboro, NC, USA, Tel: 336-285-2858; Fax: 336-500-0115; E-mail: gravesjl@ncat.edu

Submitted: 24 February 2017

Accepted: 04 March 2017

Published: 09 March 2017

ISSN: 2334-1815

Keywords

- *E. col*
- Silver
- Nanoparticles
- Resistance
- Genomics

Abstract

Escherichia coli can rapidly evolve resistance to silver nanoparticles (AgNP). Here we utilize experimental evolution to demonstrate that selection for Ag^+ resistance confers resistance to AgNPs. By generation 200, the minimum inhibitory concentration of Ag-selected increased by ~9.5-fold compared to control replicates. Ag-selected replicates also showed superior resistance to AgNPs. Genomic analysis identified candidate mutations in the silver-resistant lines including several in the gene *cusS*, which encodes a histidine kinase that senses copper and silver ions, as well as *ompR*, outer membrane protein R, and in the RNA polymerase subunits (*rpoA, rpoB, rpoC*). Molecular simulations of the common *cusS* mutations showed that they imputed greater silver ion affinity compared to that of the ancestral *cusS* sequence. This study supports the contention that the primary action of AgNPs against bacteria is the release of Ag^+ ion. Furthermore it validates that bacterial resistance to silver can occur rapidly by simple genomic changes.

ABBREVIATIONS

Ag^+: Ionic Silver; AgNP: Silver Nanoparticles

INTRODUCTION

Silver, either in ionic form (Ag^+) or as nanoparticles (AgNPs), has been shown to be toxic to many species of bacteria, including *Escherichia coli*, *Enterococcus faecalis*, *Staphylococcus aureus*, and others [1-4]. For example, silver interacts with the thiol groups in their respiratory enzymes and other proteins, causing them to become inactivated [5,6], and it binds to the cell envelope, inhibiting respiration [4,7]. In *E. coli*, at least, silver also inhibits the uptake of phosphorous and causes the release of phosphate, mannitol, succinate, proline, and glutamine from cells [2,8]. Silver ions are also thought to impede DNA replication by causing it to condense. Thus, Ag^+ ions may be detrimental or lethal because they disrupt metabolism, cell signaling, DNA replication, transcription, translation, and cell division, either directly or through the generation of reactive oxygen species [2,3]. There is still some debate concerning the action of metallic nanoparticles on bacteria. Xiu et al., 2012 reported negligible bactericidal actions of silver nanoparticles on bacteria under reducing conditions (no Ag^+ produced), whereas Bandyopadhyay et al., 2012 found that zinc oxide nanoparticles were more effective at inhibiting growth in *Sinorhizobium mellioti* than equivalent concentrations of ionic zinc oxide and Bondarenko et al., 2013 cited several studies indicating that the amount of silver released from AgNPs was insufficient to account for the observed antibacterial effect [9-11].

Owing to the multiplicity of its effects on bacterial cells, it has been proposed that it is difficult for bacteria to evolve resistance to silver, particularly in its nanoparticle form [2]. However, silver resistant bacteria have been isolated from nature [12] and one study has examined how a naïve bacterium (*E. coli* K12 MG1655) can evolve resistance to AgNPs under laboratory conditions [13]. Other studies have utilized ionic silver to isolate silver resistant strains [14,15]. Li et al., 1997 found silver resistant strains displayed active efflux of silver and were deficient in porins. Randall et al., 2015 corroborated Li et al., 1997 by demonstrating

the existence of specific mutations in the *cusS* gene [15]. This gene encodes a histidine kinase that is involved in sensing both copper and silver ions and is linked to the cus proteins responsible for efflux. Graves et al., 2015 in response to selection for AgNP resistance found mutations in *cusS* as well as in *ompR.* The latter gene is associated with porin expression. As these mutations were indels it is highly likely that they represent loss-of-function mutations and these in turn could account for porin deficiency.

As there have been few controlled studies of how bacteria evolve resistance to either Ag^+ or AgNPs, and that the studies that do exist have not used the same bacterial strains or protocols, this study examines whether similar mechanisms evolve in silver resistant bacteria generated by ionic versus nanoparticle silver. Specifically we tested whether selection for Ag^+ resistance confer AgNP resistance, and if so, to what degree the genomic foundations of Ag^+ are similar to those of AgNP resistance. Finally we investigated the functional/molecular mechanisms of Ag^+ resistance resulting from specific mutations in the *cusS* gene.

MATERIALS AND METHODS

Bacteria

E. coli K12 MG1655 (ATCC #47076) is the same strain used in Graves 2015. It was originally chosen due to its sensitivity to silver and the paucity of known silver or antibiotic resistant loci in this bacterium. There are no plasmids in this strain, and its chromosome has 4,641,652 nucleotides (GenBank: NC_000913.3) [16].

Evolution experiment

To generate the bacterial stocks utilized in this study we employed experimental evolution by serial transfer as described in Graves et al., 2015. Here silver selected 18 replicates were exposed to 100 g/L of AgNO3 as opposed to silver nanoparticles (AgNPs). Full details of the experimental protocol are given in Supplemental Methods. Every five days, after the corresponding transfers, the remainder of each population was frozen at -80° for future analysis. However, after generation 200 it was observed that long-term survival in -80° differed substantially for the ancestral strain and the controls compared to the Ag-selected replicates. Both the ancestor and controls showed 100% survival, while only 7 of the 17 remaining Ag-selected replicates survived freezing. Thus all assays conducted past generation 200 in this study utilized 5-7 Ag-selected replicates (Ag1, Ag3, Ag4, Ag5, A10, Ag11, Ag16) [17,18].

Phenotypic assays

Resistance to silver ions or nanoparticles was measured via changes in the minimum inhibitory concentration (MIC) and 24-hour (24-h) growth [full details provided in Supplemental Methods].

Genomic analysis

Whole-genome resequencing was performed to identify genomic variants associated with the greater AgNO3 resistance of the treatment populations compared to the controls. The full description of DNA extraction, sequencing, and variant calling are provided in Supplemental Methods. The SRA accession number for the raw fasta files is SRP065125. Sequence alignment and variant calling from the generation 200 samples was achieved by use of the ***breseq*** 0.24rc6 pipeline [19]. This pipeline uses three types of evidence to predict mutations, read alignments (RA), missing coverage (MC), and new junctions (JC). This algorithm can call variants by either consensus or polymorphism mode. In the former, only variants found in all the sequence reads are reported; in the latter, all variants are reported. The data in this paper are based on polymorphism mode.

In vivo characterization of cusS mutant susceptibility to silver nitrate

Graves et al., 2015 (AgNP); Randall et al., 2015 (AgNO3), found that mutations in *cusS* were associated with silver resistance. Indeed, the massive parallelism in *cusS* mutations demonstrated in this study further supported that this gene plays an important role in both Ag^+ and AgNP resistance. To test the efficacy of the specific mutations we scored in this study as anti-silver adaptations we utilized cloning and site directed to mutagenesis to evaluate each mutation (full details are given in Supplemental Methods). This was accomplished using the *E. coli* BL21 (DE3) strain which was engineered for site directed mutagenesis. BL21 (DE3) strains cells possess a single chromosomal copy of the *cusS* gene (homologous to K12 MG1655) and are used as a control to characterize growth under basal expression levels of the CusS protein. Survival curve assays for the control (MG1655 *cusS* wild type) and mutants (L12R, T14P, R15L, and N279H see Table (1) were performed and scored based on previous methods [20, details in Supplemental Methods]. Growth was then scored on a scale from 0-8 based on the highest dilution at which growth was observed and converted to percent cell survival as previously

Table 1: Selective Sweeps in the *cusS* gene.

Replicate	*cusS4*	*cusS2*	*cusS3*	*cusS4*
Ag1	**0.769**	**0.231**	0.000	0.000
Ag3	**0.700**	0.000	0.000	0.000
Ag5	**1.000**	0.000	0.000	0.000
Ag6	**1.000**	0.000	0.000	0.000
Ag8	**1.000**	0.000	0.000	0.000
Ag9	**1.000**	0.000	0.000	0.000
Ag10	0.000	0.000	**0.572**	0.000
Ag11	**1.000**	0.000	0.000	0.000
Ag12	**1.000**	0.000	0.000	0.000
Ag14	**0.520**	0.000	0.000	0.000
Ag15	**1.000**	0.000	0.000	0.000
Ag16	**1.000**	0.000	0.000	0.000
Ag17	0.000	0.000	0.000	**1**.000

Mutation frequencies for loci suggesting a strong selective sweep [f > 0.50 at generation 200] are shown for *cusS*. The mutations are identified as *cusS*1 = position 594,727,C→A, R15L (CGC→CTC); *cusS*2 = 594,731, T→G, T14P (ACC→CCC); *cusS*3 = position 593,936, T→G, N279H (AAT→CAT); and *cusS*4 = position 594,736, A→C, L12R (CTG→CGG). The *cusS*1 mutation is the most widely distributed, being found in 12 of the 17 replicates including 8 in which it fixed. The replicates colored blue survived freezing after generation 200.

described [20]; all experiments were performed in triplicate.

Molecular simulations

I-TASSER was used initially to predict the three-dimensional structure of the wild type CusS protein. [21]. The structure output from I-TASSER was then input into PyMOL [22] as the base structures and the four identified mutations (R15L, T14P, N279H and L12R) were substituted to generate CusS1, CusS2, CusS3 and CusS4 protein models respectively. These structures were refined in PyMOL to accommodate dimerization by comparing with published histidine kinases structures (PDB 4I5S, 5HQ3) and deemed our alpha structure configuration [see supplemental Figure S1]. CusS is a transmembrane protein; therefore, alternative structures were also generated using PyMOL that best represent this feature and deemed our beta structure configuration [see supplemental Figure S1].

The predicted protein structures were modeled using the molecular dynamics software GROMACS [23]. Each protein was minimized, equilibrated and simulated using the OPLS force field [24]. This molecular dynamics protocol follows our previously established methodology, and has been used successfully with small biomolecules [25]. Upon verifying the stability of the proteins in water the predicted structures were simulated in 0.5 mM Ag^+, 2.0 mM Ag^+ and 4.5 mM Ag^+ aqueous solvent environments at standard temperature and pressure. All of the CusS simulations were performed for minimum of 20 nanoseconds [ns] in an aqueous environment.

RESULTS AND DISCUSSION

Phenotypic analysis

Figure (1) shows the mean and standard error of MIC for the Ag-selected lines (N = 17) relative to the controls (N = 5) at generations 64, 100, 150, and 200 (Controls: 10 mg/L +/- 0.0; 41.66 +/- 2.15; 41.66 +/- 2.15; and 33.33 +/- 2.15. Silver-treatment: 36.23 +/- 0.98; 335.33 +/- 12.14; 313.05 +/- 12.26; and 406.05 +/- 8.88). The MIC of the ancestral *E. coli* K12 MG1655 (Generation 0) was determined to be 25 mg/L. The mean difference of the control and silver-treatment groups in each generation is highly significantly different as tested by one-way ANOVA (Generation 64, F = 12.851, p = 0.002; for generation 100, F = 10.496, p = 0.004; for generation 150, F = 11.087, p = 0.003 and for generation 200, F = 9.334, p = 0.006).

Figure (2) shows the 24-growth for the ancestor (N=2), controls (N = 5), and silver-treatment lines (N = 5) in response to increasing concentrations of ionic silver in generation 356. Both the ancestor and control show superior growth compared to the silver-selected in the absence of Ag+ (One way ANOVA, F = 48.153, p < 0.0001). However, at 50 – 500 mg/L Ag^+ the silver-selected lines show statistically superior growth (One way ANOVA, F = 162.51, p < 0.0001). From this figure, MIC for the ancestors and controls was determined as < 50 mg/L consistent with our previous measurements. Figure (3) shows the 24-growth for the ancestor (N=2), controls (N = 5), and silver-treatment lines (N = 7) in response to increasing concentrations of 10nm citrate-coated nanoparticles. Both the ancestor and control show superior growth compared to the silver-selected in the absence of AgNPs as well as from 50-75 mg/L (One way ANOVA, F =

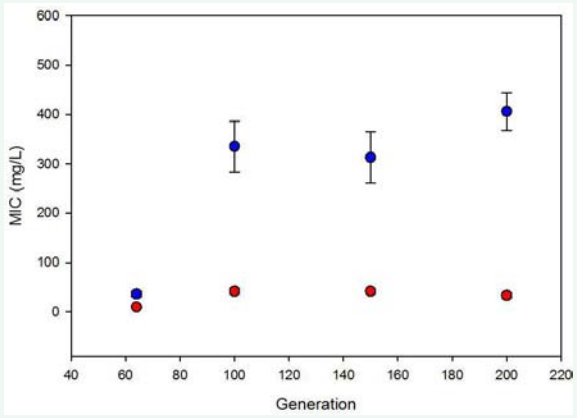

Figure 1 Minimum inhibitory concentrations (MIC) for control [red] and silver-treatment (blue) populations by generation.

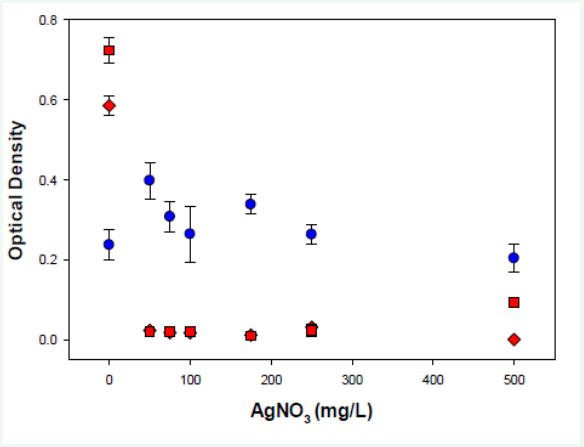

Figure 2 The mean and standard errors for 24-hour growth (N = 2 ancestor; N = 5 controls; Ag-selected) versus increasing concentration of ionic silver (Ag+) are shown for ancestor (red squares), control (red diamond) and Ag-selected (blue circles) from generation 356.

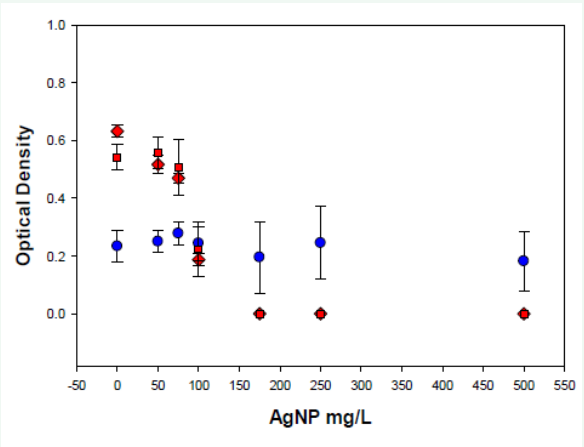

Figure 3 The mean and standard errors for 24-hour growth (N=5 controls; N = 6 Ag-selected) versus increasing concentration of silver nanoparticle (AgNP) are shown for ancestor (red squares), control (red diamonds) and Ag-selected (blue circles) from generation 356.

43.90, p < 0.0001). At 100 mg/L the ancestor, controls, and Ag-selected replicates show no difference in 24-growth. However, at 175 – 500 mg/L AgNPs the silver-selected lines show statistically superior growth (One way ANOVA, F = 4.22, p < 0.023).

Genomic analysis

We performed whole-genome resequencing to determine the differences between the ancestral strain and 200-generation samples from 5 of the 6 control populations and from 17 of the 18 silver-treatment populations (supplemental Table 2). There are a few differences between the ancestral K12 MG1655 strain used in our study and the reference genome that have been previously documented [13]; these differences are also provided here (supplemental Table 1).

We identified loci with mutations showing evidence of a selective sweep as those with frequencies (f > 0.5) at generation 200. Only four loci fulfilled this criterion in one or more of the control populations (C1-C5). These are shown in supplemental Table (2) and described in Supplemental Genomic Results. Overall, our analysis of the five control populations found a total of 38 single-nucleotide polymorphisms (SNPs), of which 36 had f > 0.05. Of these 36 most abundant SNPs, 23 were non-synonymous, 8 were synonymous, 4 were intergenic, and 1 was a non-coding mutation. There were also 22 insertion and deletion (indel) mutations, of which 16 had f > 0.05. All of the affected genes are described in supplemental Table (2).

The 17Ag-selected populations that we sequenced had a total of 100 SNPs and 29 indel polymorphisms. All of the SNPs we found had f > 0.05. Sixteen loci showed strong evidence of selective sweeps in multiple silver-selected populations. Most prominent among them were non-synonymous mutations in the following genes: *cusS*, which encodes a sensory histidine kinase that is part of a two-component system that activates expression of an operon encoding an efflux pump in response to copper or silver; *rpo*A, *rpoB*, and *rpoC* that encode subunits of the RNA polymerase; *ompR*, which encodes a cytoplasmic response regulator in another two-component regulatory system; and *yfhM*, which encodes an inner membrane-anchored lipoprotein [26].

Table (1) shows the *cusS* mutations by replicate population, the affected region of the gene, and the frequency of the allele. Thirteen of the 17 sequenced treatment populations show evidence for selective sweeps in the *cusS* gene. In 8 populations, the mutation at position 594,727 (C-T, labeled *cusS*1) went to fixation, and in 3 others that same mutation went to high frequency. Another population, Ag17, was fixed for the mutation at position 594,736 (A-C), and Ag10 shows a strong sweep (f = 0.572) for the mutation at position 593,936 (T-G). One population, Ag1, harbored both the mutation at position 594,727 and another in *cusS*, and their combined frequencies summed to unity. Three of the mutations, including the most common one at 594,727, occur before the start of the HAMP domain. This domain is ~50 amino acids long and present in histidine kinases, adenylate cyclases, methyl-accepting proteins, and phosphatases [27]. The mutation at 593,936 occurs within the active site of the His Kinase A (phosphor-acceptor) domain. It is clear that the *cusS*1 mutation was present in multiple replicates.

Table (2) shows the additional mutations (*rpo*A, *rpoB*, *rpoC*, *ompR, yfhM)* that were also present in the silver-selected treatment populations at generation 200. In Ag2, its *rpoC* mutation is found at f = 0.629 in generation 100 and sweeps to fixation by generation 200. Population Ag16 was fixed for an intergenic mutation located between the genes *pyrE* (which encodes orotate phosphoribosyltransferase) and *rph* (encodes ribonuclease PH). Populations Ag3 and Ag5 showed the same 82-bp deletion seen in the controls, while Ag9 had a unique polymorphism for a 74-bp deletion in *rph* at position 3,815,878. Finally, a 1-bp deletion was detected between *pyrE* and *rph* in population Ag14.

In vivo characterization of cusS mutant susceptibility to silver nitrate

Figure (4) reports the susceptibility of *cusS* mutants and controls to increasing concentrations of AgNO3. To account for zero survival measurements these were entered as one order of magnitude lower than the lowest observed survival of -6.00 as -7.00, as the log10 of zero is undefined. At lower concentrations (0-20 mg/L) the controls perform better than or as well as the cusS mutants. However at higher concentrations (>25 mg/L) the mutants show greater survival compared to the wild type cusS (BL21 and pET vector had 0% survivorship in this range; the treatment effect was highly significant F = 23.77, p < 0.0001. A post-hoc Bonferoni multiple comparison tests showed that p*cusS*_L12R, p*cuS*_T14P, and p*cusS*_R15L mean survival was highly significantly greater than *pcuS_WT* (p < 0.0001, p < 0.016, and p < 0.0001). The pcusS_N279H mutant showed higher % survival compared to the p*cusS*_WT but this was not statistically significantly different). These changes in growth are not due to differences in expression levels of the mutants and wild type proteins as similar expression levels were detected from all strains by SDS-PAGE (data not shown).

Molecular simulations

Figure (5) reports the number of silver ions interacting with the predicted sensory domain of each of the *cusS* mutations we identified in the silver selected replicates. The secondary structures vary little in the HAMP and kinase regions of the monomer structures. The structure has 6 beta sheets and 3 helices in the sensory domain, 3 and 1 3-10 helix in the HAMP with 6 sheets and 5 helices in the kinase region. The structure has 1 helix and 5 short sheets in the sensory domain, 2 helices in the HAMP with 4 sheets, 1 3-10 helix and 6 helices in the kinase region. It is of note that the sensory domain is more open and has a coil structure when compared to the more ordered sensory domain alpha structure (see the Supplementary Information).

The three-dimensional structure of the CusS sensor domain has recently been determined by X-ray crystallography (PDB 5KU5) [20]. We therefore compared the published structure with our simulations within the sensory domain and the overlays show that the published structure appears to share some similarities with both our alpha and beta structures. The alpha structure more closely resembles the overall 3-dimensional shape of 5KU5 and encompasses a similar overall secondary and tertiary structure (see the Supplementary information and Methods).

All CusS variant simulations were also performed in presence

Table 2: Selective sweeps in the *rpoABC, ompR, and yfhm* genes.

Replicate	rpoA	rpoB	rpoC1	rpoC2	rpoC3	ompR1	ompR2	yfhm
Ag2	0.000	0.000	**1.000**	0.000	0.000	0.000	0.000	0.000
Ag4	0.000	0.000	0.000	0.000	0.000	0.000	0.000	**1.000**
Ag6	0.000	**1.000**	0.000	0.000	0.000	0.000	0.000	0.000
Ag7	**0.064**	0.000	0.000	0.000	0.000	0.000	0.000	0.000
Ag8	**1.000**	0.000	0.000	0.000	0.000	0.000	0.000	0.000
Ag11	0.000	0.000	0.000	0.000	0.000	0.000	**1.000**	0.000
Ag12	0.000	0.000	0.000	0.000	0.000	**0.678**	0.000	0.000
Ag16	0.000	0.000	0.000	0.000	0.000	0.000	**0.870**	0.000
Ag17	0.000	0.000	0.000	0.000	**0.830**	0.000	0.000	0.000
Ag18	0.000	0.000	0.000	**1.000**	0.000	0.000	0.000	0.000

Mutation frequencies for loci suggesting a strong selective sweep (f > 0.50 at generation 200) are shown for *rpo* and *ompR*. The mutations are identified as *rpoA* = position 3,440,924, C→A, G36C (GGC→TGC); *rpoB* = 4,183,378, T→C, S712P (TCC→CCC); *rpoC*1 = position 4,186,532, A→G, K395E (AAA→GAA); *rpoC*2 = position 4,185,540, C→T, P64L (CCG→CTG); *rpoC*3 = 4,186,099 is a 9bp x 2 insertion, *ompR*1 = position 3,536,553, T→G, D11A (GAT→GCT) and *ompR*2 = position 3,536,061 is a 1-bp deletion. Of these mutations only the *rpoA* and *ompR*2 mutations are shared in two replicates.

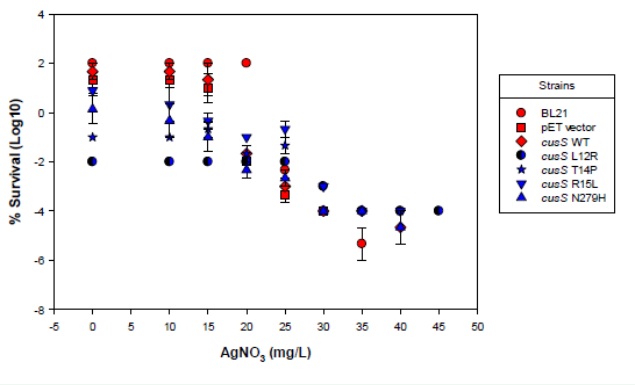

Figure 4 Log 10 percent cell survival of cusS mutants and controls in BL21 (DE3) *E. coli* cells are shown.

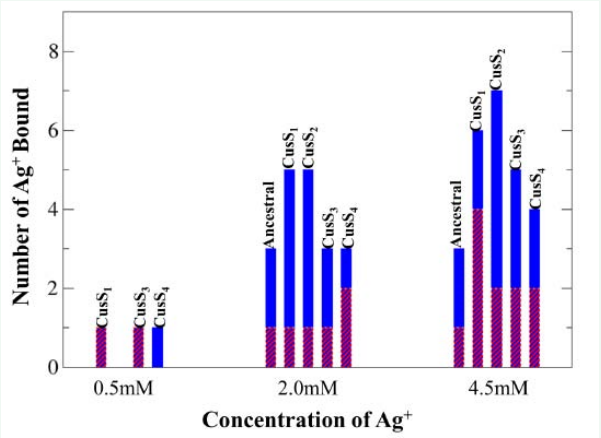

Figure 5 Number of silver ions interacting with the sensory region of each CusS dimer. The alpha structure configuration results are shown in red and the beta structure configuration results are shown in blue. The increase in Ag+ ion interactions with the sensory domain is distinctive for all mutant proteins compared to the ancestral protein. The simulations show that there is a greater interaction between silver and the beta protein configurations.

of increasing amounts of silver 0.5 mM, 2.0 mM and 4.5mM in the solvent environments. In all models, silver binding occurs within the sensory domain which is consistent with the expectations garnered in the literature [28]. Figure (6) shows the interacting residues and the number of silver ions interacting with the sensory domain for each concentration of silver. Our simulations indicate that the *CusS1* mutant in both structures have more silver ions associated with the protein when compared to the ancestral simulations. Similarly, the other mutants we tested (*CusS2-CusS4)* also showed similar or increased binding to silver. The beta structure exhibits intramolecular binding of silver ions along the dimer interface of the sensory domains see Figure (6), this was not observed in the alpha structure as the beta structure was modeled to include the multipass transmembrane region of the CusS proteins. While the membrane was not included in these simulations, binding was not observed within the predicted hydrophobic region of the protein as expected.

CONCLUSION

This study extends and corroborates our previous finding [13] that a highly sensitive bacterium, *E. coli* K12 MG1655, without any known prior exposure to silver treatment, can rapidly evolve resistance to silver. The previous study used silver nanoparticles, while in this work we utilized ionic silver. Here we demonstrate that selection for Ag^+ resistance conferred AgNP resistance. By generation 64, the Ag-selected lines already had significantly higher MIC for ionic silver compared to the controls, and this difference increased to > 9-fold by generation 200. Samples from generation 356 demonstrated that the functional response to concentration was essentially similar for Ag^+ and AgNPs, however ionic silver was more toxic to the controls (with an MIC < 50 mg/L) compared to AgNPs (MIC < 175 mg/L). We do not find this result particularly surprising as we have always suspected that the primary mechanism of AgNP toxicity is the release of Ag^+ ions. However it is also clear that the nanoparticle itself plays some role in AgNP toxicity, as evidenced by previous studies [11,29] and our own unpublished resulting demonstrating that *E. coli* has a much harder time evolving resistance to triangular shaped AgNP, as opposed to either spherical AgNPs or ionic Ag^+.

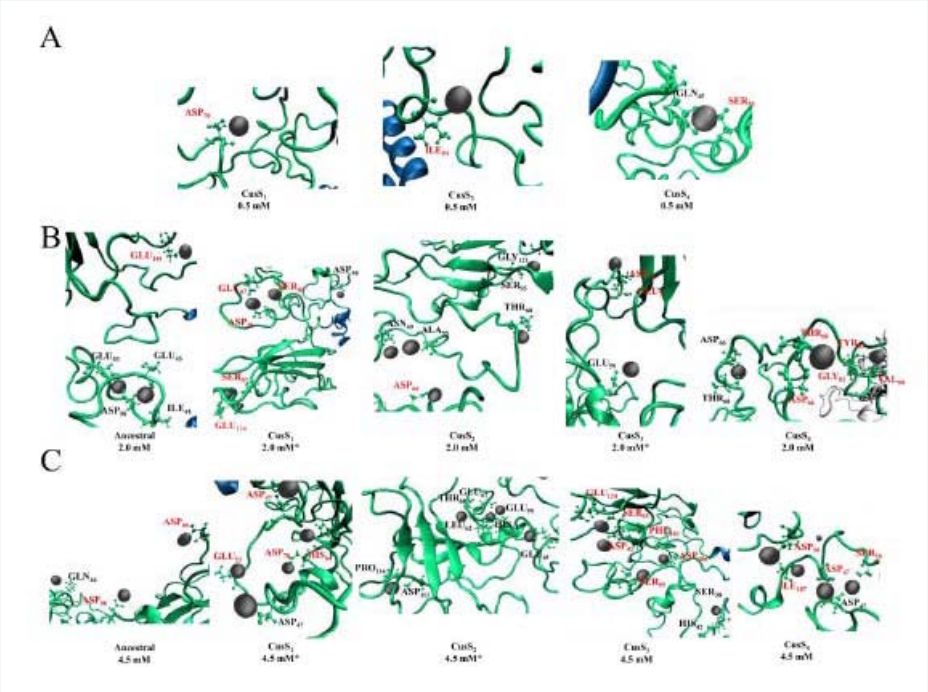

Figure 6 Final simulation snapshots of the dimeric CusS protein beta structure sensory domains bound to silver ions. The residues interacting are labeled in black (monomer 1) and red (monomer 2). A) The 0.5 mM Ag+ simulations. Binding only occurred in CusS1, CusS3, and CusS4, thus the ancestral and CusS2 are not shown. B) The 2.0 mM Ag+ simulations. Silver was seen bound in all five simulations. C) The 4.5 mM Ag+ simulations. Silver binding was observed in all simulations and as silver concentration increases there is an increase in the observed silver binding for the mutant structures.

We also found that the genomic foundations of Ag^+ resistance similar to those of AgNP resistance. Our sequencing of AgNP-resistance and Ag^+ - resistant stocks [9] have shown in both cases hard sweeps for indel mutations in *ompR* (which encodes outer membrane protein R). This protein is clearly involved in the regulation of porins, and porins have been shown to be deficient in past silver-resistant stocks as well as changes in cell wall stickiness associated with biofilm formation in *E. coli* and other bacteria [14,30-32]. In addition to *ompR*, we observed multiple selective sweeps in *cusS* and the RNA polymerase subunit proteins in the Ag-selected populations (Tables 1 and 2). In generation 200, 13 of the 17 Ag-selected populations displayed a new *cusS* mutation with frequencies over 0.50. In 9 of the 13 the mutants reached 1.00 (including one population, Ag1, in which two mutations together totaled 1.00). The *cusS1* (R15L) mutation was fixed in 8 of the 9 populations (Table 1). Interestingly enough, the *cusS*1 mutation was not observed in Ag4 but this replicate showed a combination of mutations in *yfhm* and *ompR*. Our previous study [13] also found a 7-bp deletion in *yfhm* was associated with resistance to AgNPs, suggesting that it, too, is important to silver resistant phenotypes. These results also suggest that the evolution of anti-silver phenotypes are dynamic, mean Ag^+ MIC increased by ~21% between generation 100-200. Over this period there were changes in the replicate genomes (Supplementary Tables 2 & 3). We did not sequence generation 356, but is possible that additional variants arose. Some of these may have been directly anti-silver, but many others would have been compensatory [33].

In 5 Ag-selected populations, mutations in *rpoA*, *rpoB*, or *rpoC* genes reached frequencies over 0.50, including 4 fixations; and in 3 populations mutant *ompR* alleles reached frequencies over 50%, including 1 fixation (Table 2). The *rpoA*, *rpoB*, and *rpoC* genes encode subunits of RNA polymerase. Four populations (Ag8, Ag11, Ag12, and Ag16) had fixations of the *cusS1* mutant plus fixations or near-fixations of mutations in either *rpoC* or *ompR*. Only 2 of the 17 sequenced populations in the silver-treatment group (Ag4 and Ag7) did not have fixations or near-fixations of mutations at any of these 5 loci. The *cusS1* allele was present at a low frequency in Ag7 (Table 1) however a mutation was detected in *fadB* which is involved in the biosynthesis of polyhydroxyalkanoates was detected in this replicate at f = 0.432. Overall, we saw many fixations or near-fixations affecting the same small set of genes (and in the case of *cusS* often the same position within the gene) in the treatment populations. Yet the fact that not all the replicates (Ag4 and Ag7 specifically) contained the common anti-silver mutations suggests that other mechanisms may also be in play in this adaptation.

This extreme parallelism displayed for *cusS*, *ompR*, and *rpo's* identifies these genes and their encoded functions as likely targets of selection [34,35] that caused the increased silver-resistance in the treatment populations. Moreover, there is strong corroborating evidence from a recent study by Randall et al., [15] that *cusS* and *ompR* mutations contribute to resistance to ionic silver. Using a selection protocol similar to ours, they found mutations in *cusS* (G1130A) and *ompR* (G596A) in *E. coli* BW25113. They further showed that silver resistance was lost when the evolved alleles were reverted to their ancestral state, while

resistance was restored when the evolved alleles were restored [15]. Here we utilized cloning and site directed mutagenesis to compare % survivorship in increasing concentrations of AgNO3 for wild type *cusS* and four *cusS* mutants identified by EERseq (L12R, T14P, R15L, and N279H) in a BL21 background. Using this protocol all the mutants showed superior survivorship in the highest concentrations of Ag^+ measured (L12R, T14P, R15L were highly statistically superior). These results are further supported by our molecular simulations that indicate that the mutants intereact with a greater number of silver ions at increasing concentrations.

However the Randall et al., study did not find mutations associated with RNA polymerase (*rpo*ABC) or any of the other silver-resistance associated polymorphisms we discovered. This is likely due to the fact that they did not conduct whole genome resequencing. It is known that silver negatively impacts transcription therefore it is possible that the RNA polymerase mutations found in the silver treatment lines are contributing to resistance. However, at least one *rpoB* mutation (position 4,183,817, C- A, f = 0.503) was observed in the C5 population of this study (Table S2a). Sporadic RNA polymerase mutations were also observed in the control replicates of our previous study [13] suggesting that these mutations might also have resulted from some shared feature of the control and silver selection environment (possibly sugar concentration). However it is also known that mutations in the RNA polymerase subunits are pleiotropic and these are often observed in *E. coli* experimental evolution studies [26,36]. A recent study suggests that mutations in RNA polymerase subunit genes play a key role in altering gene expression in response to stress resulting in acclimatized phenotypes which themselves become the targets of selection [37]. This is supported by our results showing that 3/9 replicates in generation 100 did not display mutations in the *cusS*, *ompR*, or *yfhm* genes, but instead displayed mutations that may have gene associated with gene expression (*rpo*'s and intergenic; Supplementary Table 3).

Finally, the design of our previous experiment [13] was incapable of addressing whether or not the increase in AgNP resistance mutations occurred by independent mutations. That experiment did not begin its replicates from independent outgrowths of single cells (i.e., colonies). In this study, we did so, meaning that mutations that rose to high frequency or became fixed were independent events. Therefore it is significant that 11/17 sequenced treatment populations showed *cusS* mutations at the same site in the gene. We take this exceptional convergence, along with the evidence from our mutagenesis and molecular simulations, as strong evidence of its utility as an adaptation to ionic silver. We are confident in excluding the possibility that this convergence of the main *cusS* mutation (position 594,727) could have resulted from accidental contamination of the replicates, as the replicates all show unique sets of rarer polymorphisms. In addition, we also observed several different *cusS* alleles that rose to high frequency. Such parallelism at the nucleotide level is not without precedent, especially in studies with strong selection under highly stressful conditions. Convergence in the long-term evolution with *E. coli* B growing at moderate temperature [37°C] often involves the same genes, but only rarely involves the exact same base changes [38]. By contrast, a study of adaptation to very high temperature [42.2°C] using the same strain and medium but at very high temperature found extensive parallelism even at the sequence level [39].

Our molecular simulations provide some explanation for the wide spread appearance of this set of *cusS* mutations. Each mutation was shown to have greater affinity for silver compared to the ancestral sequence. This may have in turn allowed these mutant proteins to have a greater impact on the activity of the cusCFBA efflux system, resulting in less intracellular Ag^+ ions, and hence less damage caused by Ag^+ ion effects.

In future work, we would like to do similar experiments with the mutation we observed in our study, including those affecting the RNA polymerase structure that were not tested in that previous study. In addition, it would be interesting to see what affects these alleles have on competitive fitness of the bacteria in the absence of silver, given the growing recognition for the importance of the fitness costs associated with resistance to antibiotics [40-42]. Indeed, the inferior 24 hour growth observed in standard medium and poor survival of the Ag-selected replicates due in -80° freezing strongly suggests that these alleles would be rapidly lost in the absence of silver. Finally, our current work only illustrates changes in the genome. To further connect the relationship of genome to phenotype we will need studies of the transcriptomic effects of these genomic changes, as we suspect many of these mutations significantly impact gene expression in response to elevated amounts of silver (ionic or nanoparticle).

ACKNOWLEDGEMENTS

Rashin Sedighi, Soodeh Baghaee-Ravari, Rachel Spencer, Herve Nonga, Quincy Cunningham, and Jaminah Norman provided assistance with the maintenance of the bacterial cultures and the MIC experiments. Jeffrey Barrick and Daniel Deatherage provided assistance with the use of the ***breseq*** computational pipeline. Richard Lenski helped in designing this experiment and gave extensive comments on earlier drafts of the paper.

FUNDING

This work was funded via support from the Joint School of Nanoscience & Nanoengineering, North Carolina A&T State University and UNC Greensboro, and by the BEACON Center for the Study of Evolution in Action (National Science Foundation Cooperative Agreement No. DBI-0939454). Any opinions, findings, and conclusions or recommendations expressed in this material are those of the authors and do not necessarily reflect the views of the National Science Foundation. We would like to acknowledge the use of high performance computational facilities at the North Carolina State A&T University during the course of the present study.

REFERENCES

1. Berger TJ, Spadaro JA, Chapin SE, Becker RO. Electrically generated silver ions: quantitative effects on bacterial and mammalian cells. Antimicrob Agents Chemother. 1976; 9: 357-358.

2. Rai MK, Deshmukh SD, Ingle AP, Gade AK. Silver nanoparticles: the powerful nanoweapon against multidrug-resistant bacteria. J Appl Microbiol. 2012; 112: 841-852.

3. Mijnendonckx K, Leys N, Mahillon J, Silver S, Van Houdt R. Antimicrobial silver: uses, toxicity and potential for resistance. Biometals. 2013; 26: 609-621.

4. Rai M, Yadav A, Gade A. Silver nanoparticles as a new generation of antimicrobials. Biotechnol Adv. 2009; 27: 76-83.

5. Feng QL, Wu J, Chen GQ, Cui FZ, Kim TN, Kim JO. A mechanistic study of the antibacterial effect of silver ions on Escherichia coli and Staphylococcus aureus. J Biomed Mater Res. 2000; 52: 662-668.

6. Liau SY, Read DC, Pugh WJ, Furr JR, Russell AD. Interaction of silver nitrate with readily identifiable groups: relationship to the antibacterial action of silver ions. Lett Appl Microbiol. 1997; 25: 279-283.

7. Klasen HJ. Historical review of the use of silver in the treatment of burns. I Early uses. Burns. 2000; 26: 117-130.

8. Yamanaka M, Hara K, Kudo J. Bactericidal actions of a silver ion solution onEscherichia coli, studied by energy-filtering transmission electron microscopy and proteomic analysis. Appl Environ. Microbiol. 2005; 71: 7589-7593.

9. Xiu ZM, Zhang QB, Puppala HL, Colvin VL, Alvarez PJ. Negligible particle-specific antibacterial activity of silver nanoparticles. Nano Lett. 2012; 12: 4271-4275.

10. Bandyopadhyay S, Peralta-Videa JR, Plascencia-Villa G, José-Yacamán M, Gardea-Torresdey JL, Comparative toxicity assessment of CeO2 and ZnO nanoparticles towards Sinorhizobium meliloti, a symbiotic alfalfa associated bacterium: use of advanced microscopic and spectroscopic techniques. J Hazard Mater. 2012; 241-242.

11. Bondarenko O, Ivask A, Käkinen A, Kurvet I, Kahru A. Particle-cell contact enhances antibacterial activity of silver nanoparticles. PLoS One. 2013; 8: e64060.

12. Silver S, Gupta A, Kazuaki M, Lo J. Resistance to Ag(I) cations in bacteria: Environment, genes, and proteins. Met based Drugs. 1999; 6: 315-320.

13. Graves JL Jr, Tajkarimi M, Cunningham Q, Campbell A, Nonga H, Harrison SH, et al. Rapid evolution of silver nanoparticle resistance in Escherichia coli. Front Genet. 2015; 6:42.

14. Li XZ, Nikaido H, Williams KE. Silver-resistant mutants of Escherichia coli display active efflux of Ag+ and are deficient in porins. J Bacteriol. 1997; 179: 6127-6132.

15. Randall CP, Gupta A, Jackson N, Busse D, O'Neill AJ. Silver resistance in Gram-negative bacteria: a dissection of endogenous and exogenous mechanisms. J Antimicrob Chemother. 2015; 70: 1037-1046.

16. Riley M, Abe T, Arnaud MB, Berlyn MK, Blattner FR, Chaudhuri RR, et al. Escherichia coli K-12: a cooperatively developed annotation snapshot--2005. Nucleic Acids Res. 2006; 34: 1-9.

17. Kedziora A, Gerasymchuk Y, Sroka E, Bugla-Ploskonska G, Doroszkiewicz W, Rybak Z, et al. Use of the materials based on partially reduced graphene-oxide with silver nanoparticle as bacteriostatic and bactericidal agent. Polim Med. 2013; 43: 129-134.

18. GE Health Life Sciences. 2014.

19. Deatherage DE, Barrick JE. Identification of mutations in laboratory-evolved microbes from next-generation sequencing data using breseq. Methods Mol Biol. 2014; 1151: 165-188.

20. Affandi T, Issaian AV, McEvoy MM. The Structure of the Periplasmic Sensor Domain of the Histidine Kinase CusS Shows Unusual Metal Ion Coordination at the Dimeric Interface. Biochemistry. 2016; 55: 5296-5306.

21. Zhang Y. I-TASSER: fully automated protein structure prediction in CASP8. Proteins. 2009; 77 Suppl 9: 100-113.

22. Schrödinger LIC.The PyMOL Molecular Graphics System, version 1.3; LLC: NewYork, 2010.

23. Hess B, Kutzner C, van der Spoel D, Lindahl E. GROMACS 4: Algorithms for Highly Efficient, Load-Balanced, and Scalable Molecular Simulation. J Chem Theory Comput. 2008; 4: 435-447.

24. Jorgensen WL. Tirado-Rives J. The OPLS [optimized potentials for liquid simulations] potential functions for proteins, energy minimizations for crystals of cyclic peptides and crambin. J Am Chem Soc. 1988; 110: 1657-1666.

25. Rhinehardt KL, Srinivas G, Mohan RV. Molecular Dynamics Simulation Analysis of Anti-MUC1 Aptamer and Mucin 1 Peptide Binding. J Phys Chem B. 2015; 119: 6571-83.

26. Conrad TM, Frazier M, Joyce AR, Cho B-K, Knight EM, Lewis NE, et al. RNA polymerase mutants found through adaptive evolution reprogram Escherichia coli for optimal growth in minimal media. Proc Natl Acad Sci. 2010; 107: 20500-20505.

27. Hulko M, Berndt F, Gruber M, Linder JU, Truffault V, Schultz A, et al. The HAMP domain structure implies helix rotation in transmembrane signaling. Cell. 2006; 126: 929-940.

28. Swapna AG, Megan M. McEvoy. The histidine kinase CusS senses silver ions through direct binding by its sensor domain, Biochimica et Biophysica Acta (BBA) - Proteins and Proteomics. 2014; 1844: 1656-1661.

29. Pal S, Tak YK, Song JM. Does the antibacterial activity of silver nanoparticles depend on the shape of the nanoparticle? A study of the Gram-negative bacterium Escherichia. Appl Environ Microbiol. 2007; 73: 1712-1720.

30. Quinn H, Cameron ADS, Dorman CJ. Bacterial regulon evolution: distinct responses and roles for the identical OmpR proteins of Salmonella Typhimurium and Escherichia coli in the acid stress response. PloS Genetic. 2014; 10: e1004215.

31. Rentschler AE, Lovrich SD, Fitton R, Enos-Berlage J, Schwan WR. OmpR regulation of the uropathogenic Escherichia coli fimB gene in an acidic/high osmolality environment. Microbiol. 2013; 159: 316-327.

32. De la Cruz MA, Calva E. The complexities of porin genetic regulation. J Mol Microbiol Biotechnol. 2010; 18: 24-36.

33. Gifford DR, Toll-Riera M, MacLean RC. Epistatic interactions between ancestral genotype and beneficial mutations shape evolvability in Pseudomonas aeruginosa, Evolution 2016; 70: 1659-1666.

34. Lok C, Ho C, Chen R, Tam PH, Chiu J, Che C. Proteomic identification of the Cus system as a major determinant of constitutive *Escherichia coli* silver resistance of chromosomal origin. J Proteome Res. 2008; **7**: 2351-2356.

35. Munson GP, Lam D, Outten FW, O'Halloran TV. Identification of a copper-responsive two-component system on the chromosome of *Escherichia coli* K-12. J Bacteriol. 2000; 182: 5864-5871.

36. LaCroix RA, Sandberg TE, O'Brien EJ, Utrilla J, Ebrahim A, Guzman GI, et al. Use of adaptive laboratory evolution to discover key mutations enabling rapid growth of *Escherichia coli* K-12 MG1655 on glucose minimal medium. Appl Env Microbiol. 2015; 81: 17-30.

37. Rodriquez-Verdugo A, Tenaillon O, Gaut BS. First-step mutations during adaptation restore the expression of hundreds of genes. Mol Biol Evol. 2015; 33: 25-39.

38. Woods R, Schneider D, Winkworth CL, Riley MA, Lenski RE. Tests of parallel molecular evolution in a long-term experiment with *Escherichia coli*. Proc Natl Acad Sci USA. 2006; 103: 9107-9112.

39. Tenaillon O, Rodriguez-Verdugo A, Gaut RL, McDonald P, Bennett AF, Long AD, et al. The molecular diversity of adaptive convergence. Science. 2009; 335: 457-461.

40. Lieberman TD, Michel JB, Aingaran M, Potter-Bynoe G, Roux D, Davis MR, et al. Parallel bacterial evolution within multiple patients identifies candidate pathogenicity genes. Nat Genet. 2011; 43: 1275-1280.

41. Lenski RE. Bacterial evolution and the cost of antibiotic resistance. Intl Microbiol. 1998; 1: 265-270.

42. Andersson DI, Hughes D. Antibiotic resistance and its cost: is it possible to reverse resistance? Nat Rev Microbiol. 2010. 8: 260-271.

Cite this article

Tajkarimi M, Rhinehardt K, Thomas M, Ewunkem JA, Campbell A, et al. (2017) Selection for Ionic- Confers Silver Nanoparticle Resistance in Escherichia coli. JSM Nanotechnol Nanomed 5(1): 1047.